DYNAMICS OF DROPLET ACTUATION OVER TRIANGULAR COPLANAR ELECTRODE

Mainak Basu[1], Vedant P. Joshi[3], Soumen Das[1,2], Sunando DasGupta[1,3]

[1]*Advanced Technology Development Centre, Indian Institute of Technology Kharagpur*

[2]*School of Medical Science and Technology, Indian Institute of Technology Kharagpur*

[3]*Department of Chemical Engineering, Indian Institute of Technology Kharagpur*

Abstract

Dynamics of droplet actuation by electrowetting on dielectric (EWOD) highly depends on the geometry of underneath coplanar electrode. In this study, zigzag motion of the droplet is achieved by strategically placing triangular electrodes array in which consistent changing of the effective contact line occurs after every switching over the Digital Microfluidic (DMF) platform. Dynamic characterization is done for the droplet based on the experimentation performed and a quasi steady state force balance approach is used to validate the experimentation with the theory. The relevant forces are the driving electrocapillary force and the resistive friction forces are hydrodynamic force, filler fluid drag force and contact line friction force respectively. A qualitative analysis of the transfer time of a droplet over triangular electrode is compared with the conventional square electrode and being evaluated separately. Power dissipation is also studied realising an equivalent RC circuit for the experimental setup which gives an overview of the heat loss during droplet actuation. This study points to the enhancement of transport rate based on underneath electrode geometry for any micro actuation based lab on chip applications.

1. Introduction

Digital microfluidics (DMF) is a technique that facilitates manipulation of small discrete droplet sitting on a composite hydrophobic-dielectric film. The transportation of droplet is governed by an applied electric potential in an array of metal electrodes located underneath of a dielectric film. Acting as micro-reactors, droplets are used for low volume biological, biochemical and lab-on-chip operations like enzyme assay[1], immunoassay[2], the point of care devices[3], DNA based applications[4], chemical reactor bed[5-6]. Other applications include liquid dispensers[7], voltage controlled fluidic switches[8], electrostatically focused liquid lenses[9], electronic paper display[10], and many others.

In general DMF platform is designed in two configurations: closed and open platform devices[11,12]. In closed DMF devices, droplets are sandwiched between two plates. The bottom electrode acts as the activated electrodes and the top one comprises the ground electrode. This type of configuration is capable to perform primarily four different microfluidic operations like dispensing, splitting, merging and transporting[13]. On the other hand, single plate open platform configuration[14] is suitable for droplet transportation and better merging & mixing, but lack in performing droplet splitting and dispensing[15].

In an open DMF platform, a sessile conductive droplet is rested over the dielectric film in such a manner that the foot of the droplet covers two adjacent underneath coplanar

electrodes. Electrostatic actuation is provided by giving electric potential to one of the underneath electrode while keeping the other grounded. This leads to a reduction in dielectric layer-droplet foot interfacial energy on top of the activated electrode, due to modulation of dielectric charges induced by applied electric field[15]. This reduction in interfacial energy gives rise to a change in contact angle of the part of the droplet sitting over the electrically activated electrode, while the contact angle remains same in the other part of the droplet over the grounded electrode. Thus, this difference between the contact angle of the two parts of a droplet over electrically activated and non-activated underneath electrodes set forth an initial momentum to the droplet[16] which is represented by well known Young's-Lippmann equation. But, from an experimental perspective due to the presence of surface micro defects, it requires a minimum actuation voltage (threshold voltage) to commence droplet actuation by overcoming the force generated due to surface pinning[17]. This difference between the variations of the advancing contact angle and receding contact angle generates a capillary force in the direction of the activated electrode which facilitates droplet motion.

There is no predefined geometric shape for designing the underneath coplanar electrodes used in digital microfluidics. But, conventionally many researchers have successfully designed DMF platform using square coplanar underneath electrodes for performing droplet actuation[18], as DMF performance largely depends on the geometry of the underneath coplanar electrodes[19,20]. To achieve smooth high velocity with better performance, various research groups have tried out different types of driving electrodes like jagged, crescent, twin plate[21,22,23] notably mentioned. Among them, interdigitated jagged coplanar electrodes turned out to be the best in performing different lab-on-chip operations[24]. Reported articles suggest that jagged electrodes perform well for smooth droplet merging and splitting, while crescent electrodes studies report for higher droplet velocity, thus increasing the performance in transport frequency for the DMF device.

In this paper, a new fabrication platform is presented to perform droplet actuation using electrowetting on dielectric (EWOD) by strategically placing an array of triangular coplanar electrodes which results in the two directional zigzag motion of the droplet which might be helpful in droplet mixing applications. The instantaneous velocities, acceleration, and average transfer frequencies are measured and the enhancement in dynamic characteristics is quantified. A theoretical model based on a force balance approach has been developed to take into account the forces present. The model is used to corroborate the experimental data and to examine the behavior of forces at raised voltages.

2. Experimentation and methods

Experimentation is carried out by actuating a sessile conductive liquid droplet over the fabricated triangular coplanar electrode array based DMF platform. Methods to carry out this experimentation include electrode array design and fabrication, development of hydrophobic-dielectric layer, testing setup for droplet actuation and capturing droplet motion using high-speed camera connected to data acquisition system. Details of each section are presented as follows:

2.1 Electrode design

A single array consisting of nine numbers of identical electrodes of the equilateral triangular geometry of side length 1.5 mm is designed to act as control electrodes for actuation of the microdroplet. Each electrode is aligned at 180˚ orientation with each other and placed at a uniform gap of 60μm as schematically shown in Figure 1(a). Each control electrode is individually connected via a thin metal line to the contact pad of dimension 1×1 mm^2 located along the periphery of the DMF device for providing external electrical connections. The entire design is carried out using Clewin 5 design software and then implemented on an optically sensitive 4-inch chrome glass plate using an in-house laser pattern generator (Microtech Systems Inc.) facility. Optically patterned triangular electrode array on glass plate will act as photomask in subsequent photolithography process to transfer the 2-D design data on a hardware platform. Figure 1(b) shows the reflected mode optical photography of microfabricated equilateral triangular control electrode array photomask and figure 1(c) represents the original image of the DMF platform compared with standard coin for scaling.

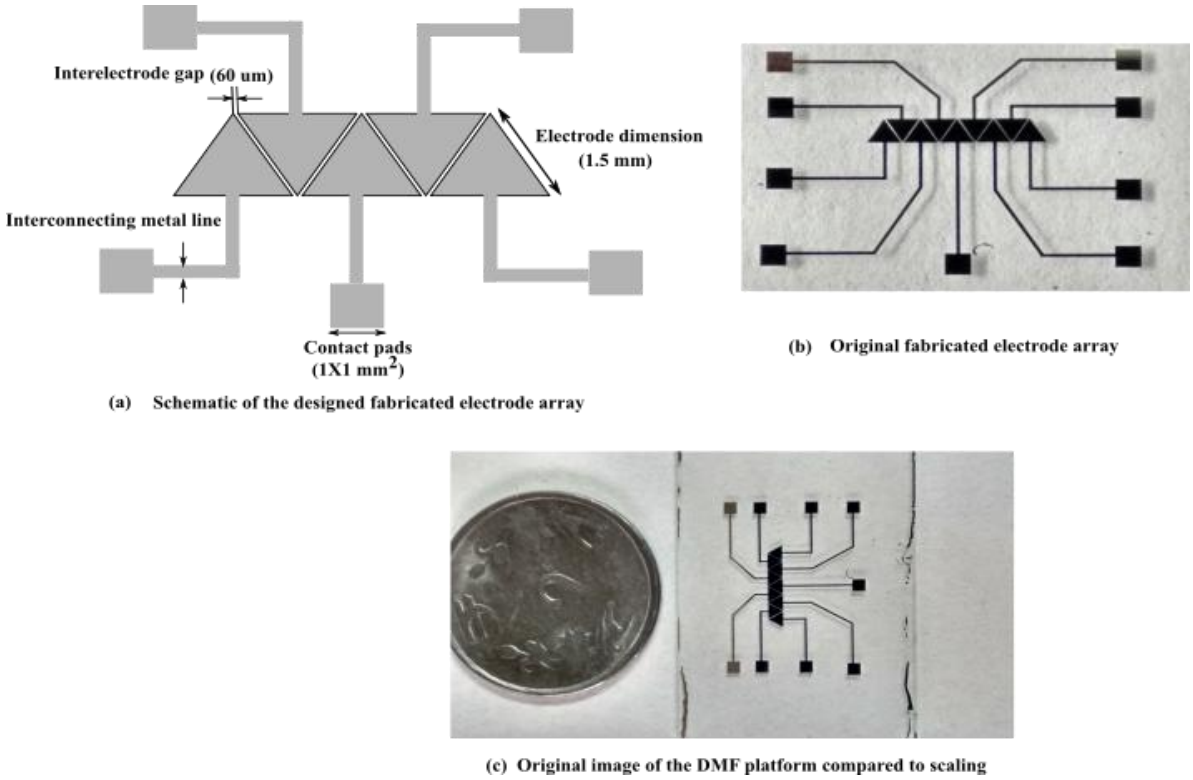

Figure 1: (a) Schematic view of the designed triangular electrode array with an individual contact pad and (b) reflected mode optical photograph of a portion of fabricated DMF platform showing an array of patterned triangular electrodes with interconnecting line and bond pads on a transparent glass substrate; (c) represents the original image of the DMF platform compared to scaling with coin.

2.2 Device fabrication

In this study, the DMF platform consists of PDMS and Teflon as a dielectric-hydrophobic layer along with underneath coplanar triangular electrode array. To initiate the fabrication process, glass slides were thoroughly cleaned in 1:1 Piranha solution. Thermal vapor deposition technique is used for coating thin film of aluminum of thickness 200±10 nm over

the cleaned glass slides. The triangular coplanar electrodes are fabricated on the aluminum layer by photolithography process, using a positive photoresist (SPR-504) and the already fabricated photomask. This is followed by wet chemical etching of exposed aluminum film and removal of remaining photoresist to complete the entire fabrication process.

Due to the easy availability and chemical inertness, Sylgard 184 (PDMS; Dow Corning; USA) is used as the hydrophobic dielectric layer with dielectric constant (ε_p = 2.7) on top of the aluminium electrode surface. The PDMS polymer is prepared by mixing the base polymer with the crosslinker in the weight ratio of 10:1 and was thoroughly degassed. Subsequently, the PDMS mixture is poured over the fabricated coplanar electrodes and spin coated (Spin Coater: Laurell Technologies Corporation) following the two-step process. In the first step the spin speed is maintained at 600 rpm for 30 sec, and in the second step, it is maintained at 6000 rpm for 60 sec with an acceleration of 4000 rpm/sec^2. The connection pad region of all the electrodes is protected with a strip of parafilm (Pachinery Plastic packaging, USA) during PDMS layer spinning process in order to keep those metal bond pads regions exposed for subsequent electrical connections. The spin coating process is followed by careful removal of the parafilm strip from the connection pads. Subsequently, the sample was kept for overnight at 98˚C in the air for completion of the polymerization process. Thickness (d_p) of the cured PDMS thin film layer was around 10±2 μm as measured by a surface profilometer (Dektak, Brukers). Cured PDMS film is further coated with an ultrathin layer of Teflon AF (3% w/w) prepared from amorphous fluoropolymer (Teflon AF 1600, Dupont) in FC-40 (Acros Organics, USA) to develop the super hydrophobic surface. Teflon(dielectric constant ε_t=2.2) solution is spin coated over the PDMS film at 3000 rpm for 30 sec to achieve a thickness (d_t) 100±20 nm. Teflon ultrathin layer is further cured in two steps: first at 110˚C for 10 min, and followed by curing at 180˚C for 20 min. During the Teflon coating process, the contact pad was again protected by a strip of parafilm as followed in the previous step. Details of step by step fabrication process are given in supporting information figure **S1**.

2.3 Testing setup

An electronic test setup was indigenously built for the generation of the desired actuation voltage and sequential activation of the electrode array to perform droplet actuation. As schematically shown in figure 2(a) the entire setup consists of fabricated DMF connected to electronic circuit board and high voltage power supply along with a high-speed camera interfaced with a computer for droplet image acquisition. The electronic circuit board consisting of Arduino Uno as a microcontroller as shown in figure 2(b), is connected to high voltage power supply module at one end and to DMF platform through electromagnetic relays on other side with suitable internal connections. Photographs of entire original setup is represented in figure 2(c).The fabricated DMF platform with nine coplanar triangular electrodes is fixed on a PCB and individual contact pads are connected to PCB using thin copper wire by conductive silver paste (Alfa Aesar: sheet resistance <0.025 ohm/square @0.001 inch thick and soldered with PCB). The microcontroller controlled programming relay board is connected to the triangular electrodes located at DMF platform for sequential activation of electrodes in an automated manner. An external electrical power source (DC power supply; Keithley instruments: 0-1kV) is connected to the relay board to supply

required voltage for droplet actuation. A high-speed camera (IMPEREX: VGA 210 camera) connected with a macro lens (IMPEREX: IPX-VGA210-L) is placed vertically above the DMF platform at a distance of approximately 30 cm to capture the droplet deformation and movement due to voltage excitation at 120 fps and connected to the computer for further processing of image data as shown in figure 2 (a). DMF platform is illuminated by a light source placed at a suitable location near the platform for clear visualisation.

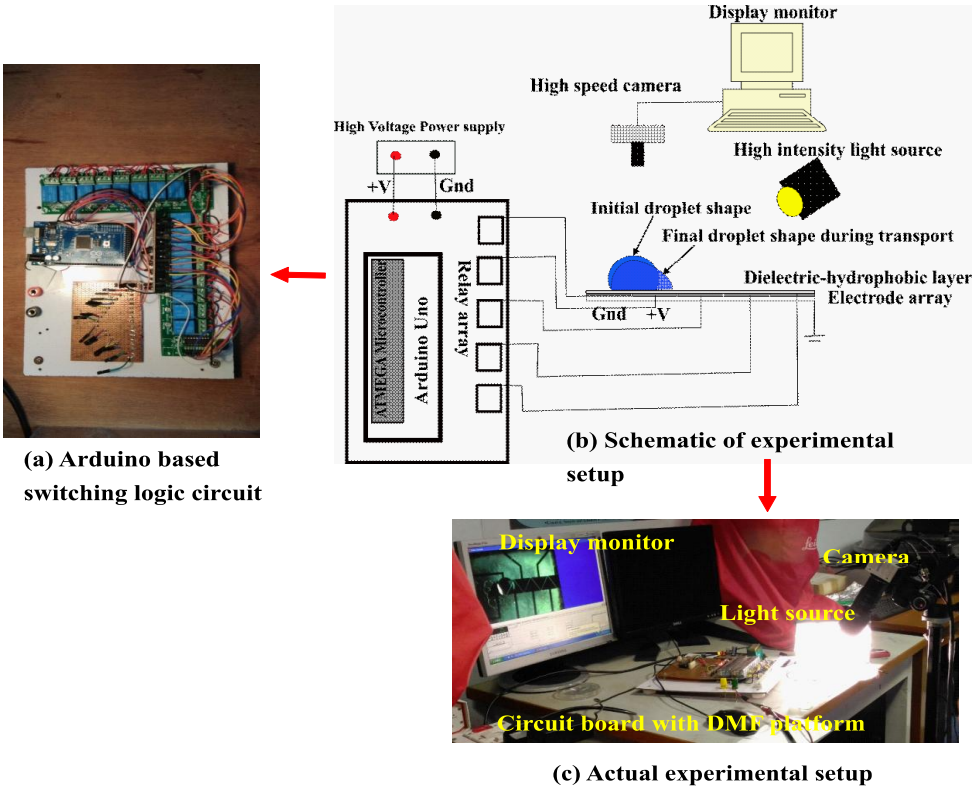

Figure 2: Entire experimental setup for performing micro droplet actuation; (a) represents the Arduino based switching logic circuit, (b) represents the schematic of the entire experimental setup, and (c) actual experimental setup.

2.4 Sequence of electrode actuation and observation of droplet movement

Experiments are performed with aqueous 1mM potassium chloride (KCl) solution droplet with optimised of volume 4±1µl prepared with Milli-Q ultrapure distilled water (Millipore India Pvt. Ltd.). Figure 3(a) and 3(b) represents the top schematic view and micro-photograph of a sequence of droplet position over DMF platform and corresponding switching logic conditions for sequential activation of electrodes. The droplet is manually dispensed over the hydrophobic surface of the DMF platform using a micropipette; in such a manner that the droplet footprint must partially overlap two adjacent coplanar triangular electrodes as schematically shown in figure 3(i). Before initiating of droplet movement, all the electrodes were in zero potential or grounded. Subsequently, voltage (*V*) is applied in between the first two adjacent coplanar electrodes to start droplet actuation, by activation of the relay 1 programmed by the microcontroller, enabling electrode 'II' at positive potential and electrode 'I' at the ground as shown in figure 3(ii). It has been observed that with the gradual increase of *V*, the 4µl volume of small single droplet starts actuation above 175 V potential.

Careful observation reveals that while entire droplet moves from the region of electrode I to activated electrode II, some part of the droplet also spill over the next adjacent grounded electrode III as represented in figure 3(iii). At this moment electrode III is activated to the desired potential via microcontroller operated relay and entire droplet starts moving towards electrode III. Therefore, forward transportation of liquid droplet occurs towards the actuating electrode as they are sequentially activated. From the three sequential photographs of droplet position as presented in figure 3(b), it may be observed that while droplet transports from grounded to activate electrodes, a portion of the droplet always moves beyond the base of the activated triangular electrode. Since relative orientation of consecutive two electrodes is 180˚, forward movement of droplet occurs in the zigzag path following orientation of electric field. Video image of droplet motion is given in supporting information figure **S2**. The above experiment is repeated for four different actuating voltages at 200V, 250V, 300V, and 350V respectively. In all cases, dynamic characteristics involved during droplet actuation are studied by recording the actuation phenomenon using the high-speed camera and subsequently analyzed through open source image processing software named 'Tracker'. After the video being recorded, frames are segmented and the displacement of the droplet is tracked from its initial position and the dynamic characteristics like displacement (*d*), velocity (*v*) and transfer frequencies (*f*) are evaluated.

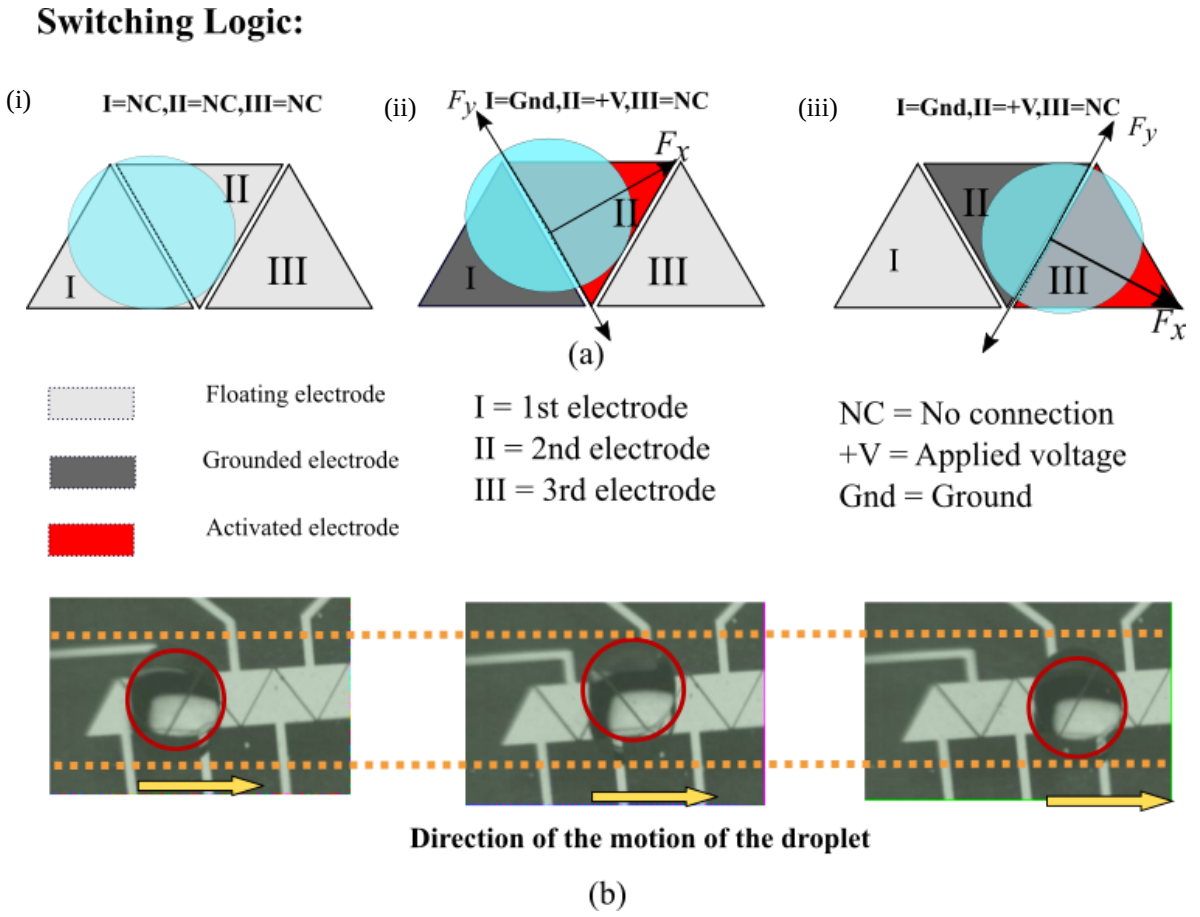

Figure 3: (a) Schematic view and (b) microphotograph of experimentally observed droplet position on coplanar triangular aluminum electrodes at three different switching logic during the transport process; (i)

initial droplet position, (ii) droplet position after 1st switching, (iii) droplet position after 2nd switching; logic condition at three different switching states are also presented.

3. Theory

A quasi-steady state force balance approach between the droplet actuating force and the resistive forces are equated to evaluate the velocities at different applied voltages. The relevant forces are the electrocapillarity inspired driving force (F_x) and the resistive forces namely, the hydrodynamic shear force (F_h), and the contact line friction force (F_{cl}) respectively. The moving droplet also suffers damping forces due to the surrounding medium. Since the filler medium is air, it is expected that the damping force is relatively weak and can be neglected as followed in previous studies [25,26] for similar conditions. It is to be noted here that the effect of gravity and inertial forces are neglected. This is because the Capillary number, Bond number, and Weber number for a droplet of volume 4±1µl (R' = 0.96 mm, where R' is the radius of the droplet) are found to be in the range of 1.99×10^{-5} to 9.50×10^{-4}; 0.257 and 5.26×10^{-5} to 1.19×10^{-3} respectively. Thus, the droplet can be considered as spherical in nature. Therefore, at quasi-steady state the driving force must be equal to all the opposing force, i.e.

$$F_e = F_h + F_d + F_{cl} \tag{1}$$

where, F_e = driving electrocapillary force, F_h = hydrodynamic force, F_d = filler fluid drag force, F_{cl} = three phase contact line friction force.

The triangular coplanar electrodes are oriented in a manner that the two adjacent electrodes form a parallelogram. The droplet is placed in such a way that the foot of the droplet touches two electrodes. When potential difference is generated between two electrodes, due to the change in interfacial tension, the droplet experiences a net force in a direction perpendicular to the shorter diagonal as shown in the schematic of figure 5. Contact line (l) is that imaginary line over which the electrocapillary force is acting underneath the droplet. Once the droplet is in contact with the activated electrode, the l is represented as,

$$l = 2\cdot\sqrt{2rx - x^2} \tag{2}$$

where r is the droplet foot radius and x is the length of the portion of the droplet in contact with the activated electrode. By repeated experimental optimization, we have observed that $x_0 = 0.2l$, where x_0 is the portion of the droplet which is initially in contact with the activated electrode. It is observed that the maximum effective contact line is happening when $x = r$, i.e. $l_{\max} = 2r$.

This phenomena repeats in each and every switching during the droplet transportation and gives rise to the zigzag motion of the droplet over the entire electrode array. In EWOD devices, droplet motion occurs as a result of capillary force which originates from the apparent wettability gradient between the actuated and non actuated electrode. The capillary line force density on the triple line (i.e. the contact line between the droplet, the substrate and the surrounding medium) can be represented as[17],

$$f_a = \gamma_{LV}(\cos\theta_V - \cos\theta_0) \tag{3}$$

From equation 3, it can be shown that capillary force acting on the droplet in the *x* direction (unit vector i) can be found from figure 4 as,

$$F_a = \int_l \gamma_{LV} \left(\cos\theta(V) - \cos\theta_0\right) dl\vec{n}\cdot\hat{i} \tag{4}$$

where *dl* is the unit element of the droplet contour line and *n* is unit normal to the contour line. Integrating equation (4), we get

$$F_a = \gamma_{LV}(\cos\theta(V) - \cos\theta_0)\int_l dl\vec{n}\cdot\hat{i} = l\gamma_{lv}(\cos\theta(V) - \cos\theta_0) \tag{5}$$

Since the hydrophobic dielectric layer takes a finite time to get charged[16], after the activation of the actuation electrode, a time-averaged transient electrical driving force is presented here. This is due to the electrocapillarity induced solid-liquid interfacial tension between the activated and ground electrode. The transient electrical driving force is averaged over the charging time period (t_c =2.3RC)[16] of the device, where saturation of the dielectric layer happens by theoretically considering an equivalent RC circuit.

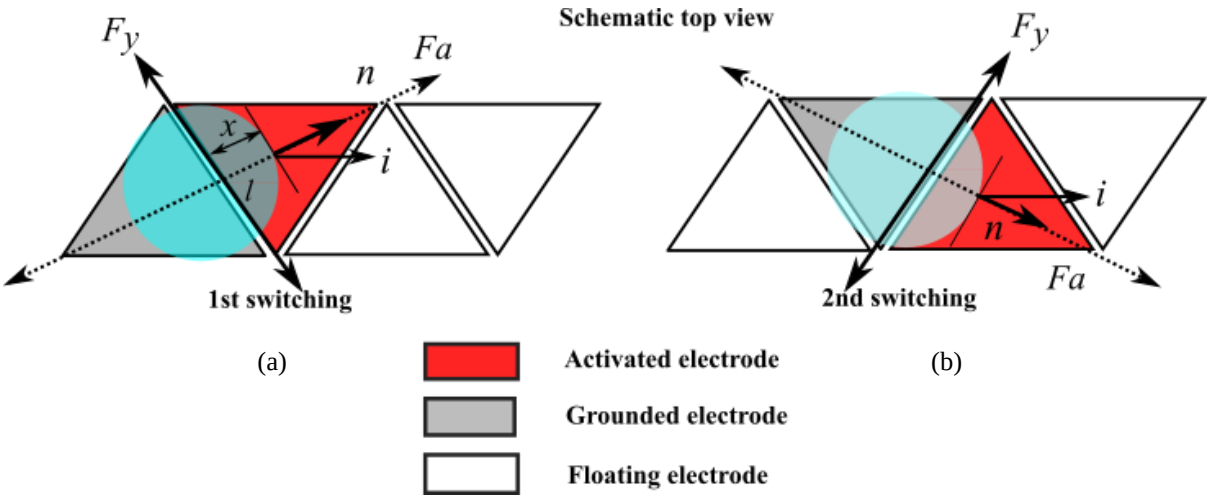

Figure 4: Schematically representing the electrocapillary force acting on the droplet diagonally due to the typical triangular geometry of underneath coplanar electrodes; (a) representing for 1st transfer and (b) for 2nd transfer (the reference coordinate system changes in each transport).

This time-averaged electrocapillary induced driving force can be written[16,17,27,25] using Young's Lippmann equation[28] as,

$$F_a = l\gamma_{LV}\left(\cos\theta - \cos\theta_0\right) = \left(\frac{lC_{eq}}{2t_c}\right)\int_{t=0}^{t=t_c}[V_{eff}(t)]^2 dt\,. \tag{6}$$

Here, θ is the instantaneous contact angle, θ_0 is the initial contact angle (here measured as 110.5°); $V_{eff}(t) = V_{eff}{}^0(1-e^{(-t/RC)})$ and $V_{eff}{}^0 = \sqrt{\left(V^2 - V^2{}_{\min}\right)}$; C_{eq} is the specific capacitance represented by $C_{eq} = \dfrac{\varepsilon_0}{\left(\dfrac{d_p}{\varepsilon_p} + \dfrac{d_t}{\varepsilon_t}\right)}$ and γ_{LV} is the liquid vapour surface tension (here measured as 70.01 mN.m). Here *R* is the series resistor along with the resistance offered by the droplet

and C is the total capacitance offered by the droplet-dielectric interface over the DMF platform. Moreover, incorporation of V_{eff}^{0} instead of V attributes the surface hysteresis effect into the present model[26]. This electrical triggering of the dielectric-droplet interface results in the spreading of the contact line at the three-phase contact line (TPCL) area. This increment in contact line at TPCL area increases the radius of curvature of the droplet, which is associated with the reduction of the liquid pressure at TPCL. Such disturbances at the TPCL region lead to adsorption of the liquid at the solid-liquid interface. This increment in the interfacial liquid concentration leads to a modification of solid-liquid interfacial surface tension[29]. Thus this modification of surface tension in two directional droplet actuation towards the activated electrode results in a zigzag manner due to the consistent changing of the effective contact line after every switching.

Hydrodynamic force appears as frictional force during droplet actuation. This friction force is generated from the solid surface (here PDMS-Teflon) at the foot of the droplet towards the liquid droplet as,

$$F_h = \frac{3\mu_f \pi r^2 u}{4h}. \tag{7}$$

Here, μ_f represents the dynamic viscosity of the liquid droplet and is taken as 8.9×10^{-4} Pa.s, r is the radius of the foot of the droplet, h represents the height of the droplet during its transportation and u is the velocity of the droplet. Considering θ_V as the change in contact angle at different applied voltages (see supporting document for variation of ϕ and its corresponding r and h value at different applied voltages), the radius (r) of the droplet can be written as,

$$r = \left[\frac{3\forall \sin^3\theta_V}{\pi(2-3\cos\theta_V+\cos^3\theta_V)}\right]^{\frac{1}{3}} \tag{8}$$

where, $\forall$ is the volume of the droplet (in this case 4μl). Corresponding h can also be calculated from the above information as,

$$h = r\left(\frac{1-\cos\theta_V}{\sin\theta_V}\right). \tag{9}$$

The droplet will experience a drag force by the filler fluid medium as its starts actuation. Under this condition, the filler fluid medium (in this case air) will form a barrier between the droplet and the surface, and thus acting as an opposing force. The drag force can be expressed mathematically as[30],

$$F_d = \frac{1}{2}C_D\rho_f u^2 A_p. \tag{10}$$

Here, ρ_f (here taken as 1 kg/m^3) and C_D are the filler fluid medium density and drag coefficient[27]respectively C_D can be expressed as,

$$C_D = 0.59 + \frac{3.4}{Re_D^{0.89}} + \frac{0.98}{\mathrm{Re}_D^{0.5}} - \frac{2\times10^{-4} Re_D}{1+3.64\times10^{-7} Re_D^{2}} . \quad (11)$$

where, Re_D is the Reynolds number and is expressed as,

$$\mathrm{Re}_D = \frac{\rho_f u D}{\mu_f} . \quad (12)$$

Here, D is the diameter of the cross section of the spherical segment (droplet) having maximum area. A_p is the droplet area projected to the direction of droplet motion. The area over which this drag force acts can be evaluated as,

$$A_p = r^2 \cos^{-1}\left[1-\frac{h}{r}\right] - (r-h)\sqrt{(2rh-h^2)} . \quad (13)$$

Dynamic wetting occurs as the droplet starts actuation from one position to another. This dynamic wetting can be visualised by the displacement of the three phase contact line from one position to other. Such instantaneous displacement or jump of the contact line leads to dissipation of the loss of energy at molecular level[31], though this jump is necessary for the advancement of the contact line. This gives arise to another friction force F_{cl} as the contact line friction force[31,32,33] acting on the droplet. Molecular kinetic theory (MKT) expresses the relation of the contact line phenomenon and the friction force which can be represented as,

$$F_{cl} = P\zeta u \quad (14)$$

Here, ζ is the coefficient of contact line friction (here ζ is taken as 0.04 Pa.s)[25] and P is the perimeter of the droplet. This force is acting through the contact line near the three phase contact line (TPCL) area.

Now, at quasi-steady state, replacing all the expression of the above mentioned forces in equation (1), we get

$$\left(\frac{l\cdot C_{eq}}{2\cdot t_c}\right)\int_{t=0}^{t=t_c}[V_{eff}(t)]^2 dt = \frac{3\mu\pi r^2 u}{4h} + \frac{1}{2}C_D\rho_f u^2 A_p + 2\pi r\zeta u . \quad (15)$$

Solution to equation (15), we can evaluate the expression of u as,

$$u = \frac{-\left[\frac{3\mu\pi r^2 u}{4h} + 2\pi r\zeta\right] + \sqrt{\left[\frac{3\mu\pi r^2 u}{4h} + 2\pi r\zeta\right]^2 + (4C_D\rho_f A_p)\cdot\left(\frac{l\cdot C_{eq}}{2\cdot t_c}\right)\int_{t=0}^{t=t_c}[V_{eff}(t)]^2 dt}}{C_D\rho_f A_p} . \quad (16)$$

4. Results and discussion

4.1 Evaluation of dynamic characteristics during droplet transportation

To demonstrate the dynamics of droplet transportation using EWOD technology, transportation characteristics of 1mM KCl solution are observed at different operating voltages. In each experiment voltages are applied gradually from 150 V with an increment in 5 V steps. It has been observed that, when the applied voltage reaches to 175 V, the 1mM ionic KCl droplet starts responding to the voltage by showing minor deformation in its shape, thus starts getting distorted from its equilibrium state. This threshold voltage, at which the droplet responds and initiates motion, is the hysteresis induced minimum actuation voltage (V_{min})[17,27]. In the present DMF configuration, droplet starts smooth translation towards actuated electrode when applied voltage reaches around 200V. Video analysis of droplet movement confirms that in each actuation process the droplet moves in the direction towards the base of the activated electrode, resulting in a zigzag motion along the direction of the electrode array. This zigzag path is attributed for the typical triangular geometry of the electrodes that are aligned 180˚ orientation with the previous one. Displacement of droplet in each actuation is measured by analyzing the distance traversed by the front portion of the droplet after single transport to depict the entire transport phenomena.

The advancing edge of the actuated droplet is tracked from the extracted stroboscopic images of the recorded video to evaluate the dynamic characteristics. While measuring the displacement of the droplet, the coordinate axis is aligned along the direction of the motion of the droplet in 'Tracker' for a single transport. So, as the direction of the droplet is changing in each transport and as a consequence the alignment of reference coordinates axis is also changing giving rise to its two directional motions over the entire DMF platform. Figure 4(a) represents the resultant displacement (d) of the droplet at different applied voltages. It is obvious that once the applied voltage is above the threshold voltage (V_{min}), the droplet starts moving, thus commencing the transport phenomena. This moving region for the droplet is depicted in figure 4(a) by 'droplet actuation period'. Once the droplet reaches its peak displacement for certain voltage, it gradually settles down and waits for the subsequent switching for the beginning of the next actuation. This droplet settling region is represented as the 'droplet settling period' in the right-hand side of figure 5(a). Since, the period of motion of the droplet is very short compared to that of the switching time (t_s = 1.5 s), (i.e. the time interval between the two successive transports); the entire dynamic characteristics are depicted for a time duration of 0.3 s for the convenience of graphical representation. Another important electrical time scales associated in understanding the dynamics behind a successful EWOD based droplet actuation in a DMF platform which is the charging time of the solid-liquid interface (t_c) i.e. in this case PDMS-Teflon and aqueous KCl[34]. In this present study it is observed that $t_c << t_s$. Under this criterion, it is expected that in a short time the liquid phase boundary will acquire a net charge when voltage is applied, thus shielding the liquid phase from the electric field. Due to this accumulation of net charge in liquid phase, the electrostatic forces exerted by the generated fringe field will cause spreading near the contact line, resulting in droplet actuation.

Instantaneous velocity (u) is evaluated by calculating point to point differentiation of the measured resultant displacement (d) data points. Figure 5(b) represents the instantaneous velocity profile during the actuation of the droplet at different applied voltages. This is illustrated from the graph that the peak velocity is reached once the droplet attains maximum displacement at the onset of switching and its value gradually increases with applied voltage. Once the droplet attains the peak velocity, it gradually ceases to move and comes to rest based on the generated momentum at different applied voltages. Thus, the droplet gradually attains its 'droplet settling velocity (v_s)' as shown in figure 4(b) during 'droplet settling period'. It is observed that the peak of the velocity graphs for different applied voltages gradually shifted right along the time scale. It is evident from the experiment that as the voltage increases, the acceleration of the droplet increases and as a consequence, the peak for the velocity curve is attained earlier for higher voltages.

The average transfer frequency (f) is the rate at which a droplet traverses an electrode pitch length L'=1.56 mm with its average velocity during a single transfer[35]. This depicts the average transport characteristics of the droplet at different operating voltages. Thus, f can be represented as $f = \frac{u_{avg}}{L'}$, as shown in figure 5(c). The red column plot represents the average transfer frequencies of the droplet for a single transport. It is obvious from the fact that transfer frequency depends on average velocity of the droplet. Thus within a dielectric breakdown regime, the increase of average velocity will result higher average transfer frequencies. As these values of f get repeated in each and every transport, this characterization helps us to understand the entire transport performance of the fabricated DMF platform.

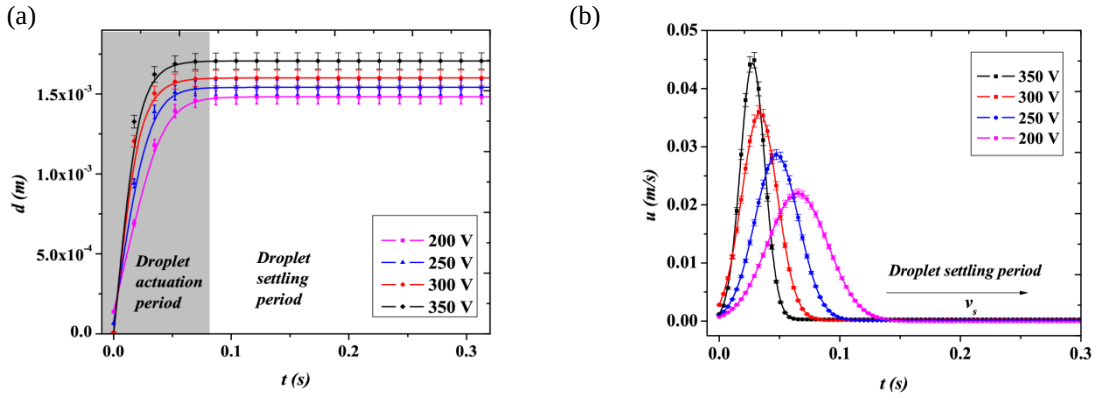

(c)

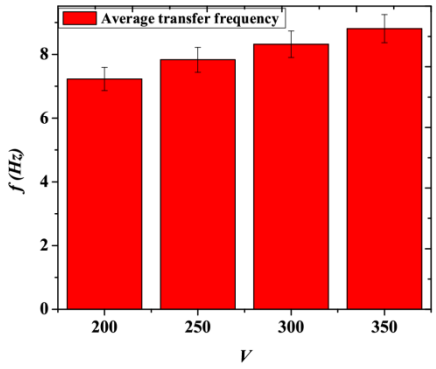

Figure 5: Dynamic transport characteristics of at four different operating voltages (200V, 250V, 300V, 350V); (a) variation of the displacement of 1mM ionic KCl at different operating voltages after 1st transport separating the droplet actuation period and the droplet settling period (best fitted curves are presented); (b) variation in the instantaneous velocities of 1mM KCl at different operating voltages after 1st transport (best fitted curves are presented); (c) depicts the average transfer frequency of the droplet during actuation at different operating voltages (±1-4% error is associated with each experimental value).

The theoretical predicted values of as evaluated from equation (14) and the experimentally measured values of u_{avg} are presented in figure 6. It is to be noted that using the experimental measured parameter values, the physics of the process is satisfactory and the trend in the values of u_{avg} at different elevated applied voltage can be understood.

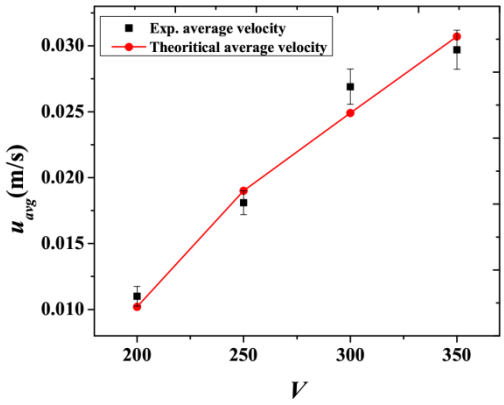

Figure 6: Comparison of the predicted and experimental average velocities at different applied voltages (±1-4% error is associated with experimental average velocity measurement).

4.2 Qualitative comparative analysis of triangular and square electrode:

Now, the time taken by a droplet to traverse effective pitch length (a) for a certain application of V is known as droplet transfer time (t_{tr}). It is observed that the major difference between the conventional square electrode and the mentioned fabricated triangular electrode is in t_{tr} for a single transfer. Figure 7 represents the schematic top view comparison of the transport of a sessile droplet of same volume over triangular as well as square electrode for single transfer. The left section and right section represents the droplet sitting over triangular and square coplanar electrode array in a EWOD based DMF platform. The droplets are placed in

such a way that the foot radius of the droplet is touching both the activated and the adjacent grounded electrode. The length (L) and inter-electrode gap (p) for both type of electrode are kept as same (here, L is kept as 1.5 mm and p as 60 μm respectively). Now, it is mentioned earlier that the droplet traverses a zigzag path over triangular electrodes and a linear path of the square electrode. It is evitable from figure 7 that the droplet follows the median of the equilateral activated electrode in case of the triangular electrode and follows the side of the square electrode to reach its effective pitch length. The effective pitch length traversed by the droplet in a single transfer over triangular activated electrode can be represented as, $a = \left(\frac{\sqrt{3}}{2} \cdot L \right) + p$ and that for square electrode can be represented as, $a' = L + p$ respectively. Thus, to traverse the effective pitch distance, the droplet must attend the average velocities (u_{avg}) at respective voltages. These u_{avg} are almost same in order for the droplet over triangular and square coplanar electrode. Qualitatively, it can be understood from the discussion that the effective pitch distance covered for triangular is less than the square electrode. Thus, it can be conclude that t_{tr} will be less in triangular as compared with the square one, i.e. the droplet completes the entire transfer much earlier in case of triangular electrode for certain applied potential after single transfer. The qualitative analysis of the t_{tr} is given below in table 1.

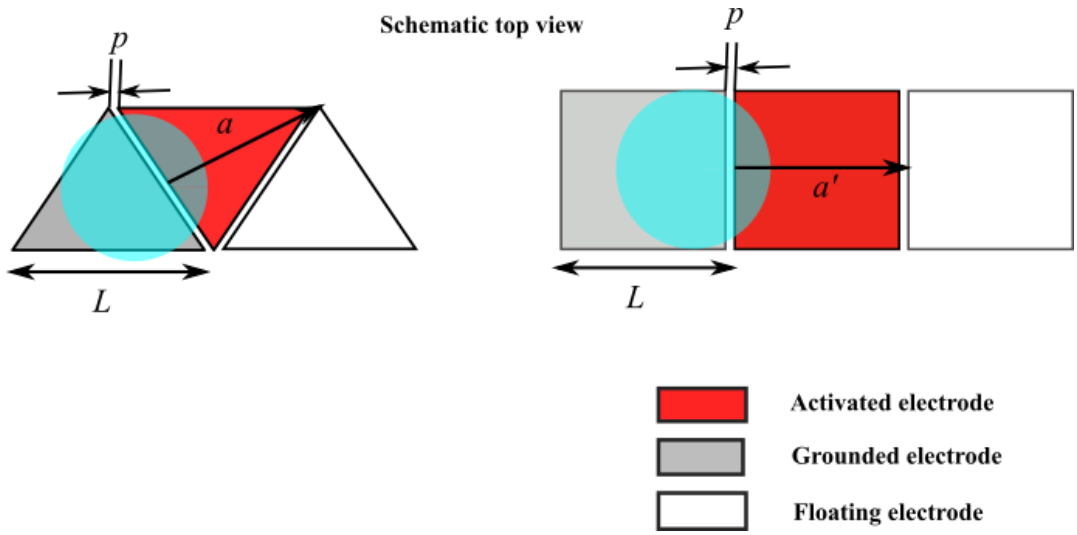

Figure 7: Comparison of **s**chematic representation of the distance covered by the droplet over triangular and square coplanar electrode array in single transfer.

Table 1: Variation in transfer time of a droplet for actuation over triangular and square coplanar interdigited electrode

Voltage (V)	Triangular electrode (present study) (t_{tr}) (s)	Square electrode (t_{tr}') (s)
200	0.8660	1
250	0.7177	0.8287
300	0.4921	0.5682
350	0.4374	0.5051

Thus, as the t_{tr} taken for a droplet to actuate over triangular electrode is less than that of square electrode, it can be stated that the rate of any actuation operation will be faster as compared to square electrode.

4.3 Force analysis:

The variation of driving force and the other acting frictional forces are shown in figure 8. It can be observed that the driving force is increasing with the increase value of applied voltage, reaching maxima at highest applied voltage, following the trend of experimental measured average velocity. This sudden increase in the driving force at higher applied voltages (i.e. 300V and 350V) might occur due to the gradual accumulation of charges in the dielectric material during the experiments performed at lower voltages. Accumulation of charges due to application of voltage at TPCL region manifests the change in contact angle, which in return develop a pressure difference inside the droplet, which results in the actuation of the droplet. However, the interesting fact that being revealed by this force analysis is the dominancy of the contact line friction force over the other frictional forces namely hydrodynamic force and drag force respectively.

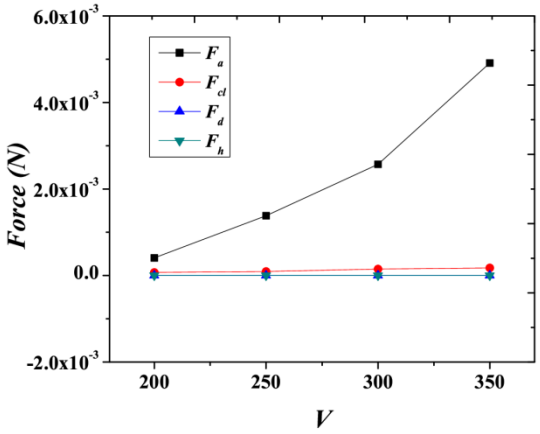

Figure 8: Forces acting on the droplet at different applied voltages.

4.4 Power dissipation:

The opposing frictional forces acting on the droplet during its motion results power loss. The resistance offered by the droplet due to applied voltage is responsible for the production of heat. The dissipation of heat due to the frictional losses is inevitable but heat generated within the droplet could be extracted to perform some useful work. The average power loss due to frictional forces can be evaluated by,

$$P_{fr} = \left(F_{sh} + F_{cl}\right).u_{avg} \tag{17}$$

The equivalent circuit of the EWOD system is shown in figure 9(a) where R and C_{eq} are the resistance of the droplet and equivalent capacitance of the dielectric hydrophobic layer. As mentioned earlier, initially the droplet is placed such that it touches both the actuated as well as the grounded electrode. We have defined a time interval from $t = 0$ to $t = t_m$ (where t_m

corresponds to the time at which the velocity of the droplet becomes maximum) from the experimental velocity data over which the driving force is active during the transport phenomena. For $t>t_m$, there is no driving force on the droplet.

The motion of the droplet can be divided in two phases; first phase corresponds to $t<t_m$ while the second corresponds to $t>t_m$. During the first phase of the droplet motion, as we can see from figure 9(a), switch is closed. The capacitor gets charged and stores some energy while some amount of heat loss occurs across the resistor (i.e. droplet). The average power loss across the resistor could be given as,

$$P_R = \frac{1}{R}\int_{t=0}^{t=tm} V_{app}{}^2 . e^{-2t/RC} dt \cdot f \tag{18}$$

During the second phase of the droplet motion, switch is open. Since no current flows through the circuit during this, there is no heat loss across the resistor i.e. no heat generation within the droplet. Figure 9(b) represents the total power dissipation across the realised resistor for the formed R-C circuit in the EWOD based DMF platform. It has been intuitively observed that as the driving voltage increases (towards 350V), the heat dissipation across the resistor also increases which results in a higher power dissipation across the R-C circuit in the DMF platform. This characterization will help in understanding the limitation of this fabricated DMF platform in performing any micro chemical reactions over such platform.

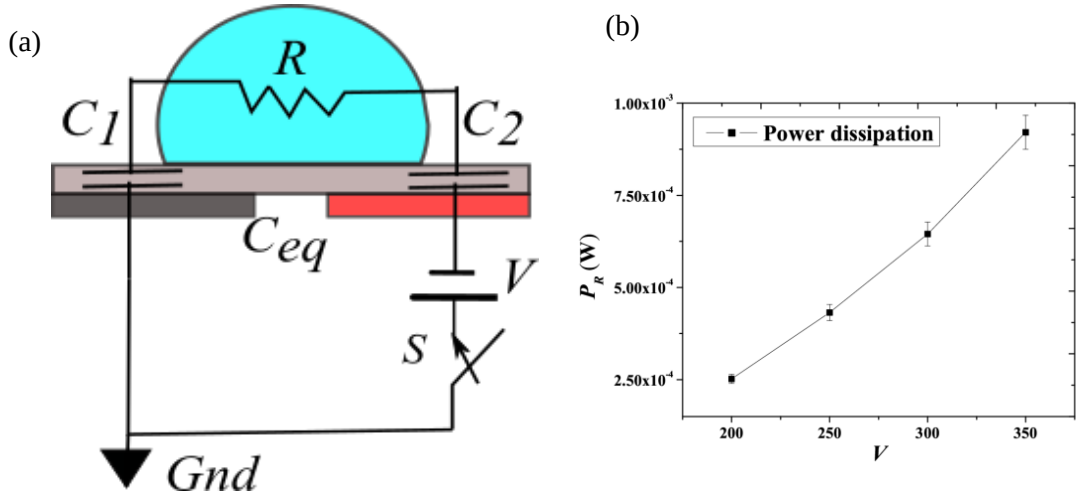

Figure 9: (a) Represents the equivalent circuit diagram for the EWOD system, where *R*, C_{eq}, *V*, *S* and *Gnd* represents the resistance of the droplet, equivalent capacitance formed from C_1 and C_2, *V* is the applied voltage, *S* is the switch of the circuit and *Gnd* represents the grounding of the circuit; (b) represents the total power dissipation across the realised resistor for the formed R-C circuit in EWOD system (±1-4% error is associated with experimental value).

5. Conclusion

Reduction in the transfer time of a droplet actuation over triangular coplanar electrodes than those of conventional square electrodes are observed and accurately measured. The transfer time of a droplet over triangular electrode and square electrode is observed to be 0.866 s and 1 s at 200V to 0.437 s and 0.5051 s at 350V respectively. This new type of fabricated triangular electrode give rise to zigzag motion of the droplet due to consistent changing of the

contact line, rather than linear motion as observed for square electrodes. A force balance approach based on the driving and resistive forces have been developed and the resulting equations are used to support the experimental results. The dominancy of the contact line friction force over the other frictional forces is also well understood. Finally, power dissipation is also evaluated at different applied voltages considering the droplet dielectric interface as an equivalent RC circuit. These results may help in developing much faster rate micro-actuator for any lab on chip applications.

References:

1. Srinivasan, V., Pamula, V. K. & Fair, R. B. An integrated digital microfluidic lab-on-a-chip for clinical diagnostics on human physiological fluids †‡. (2004).

2. Tsaloglou, M. & Morgan, H. A FLUOROGENIC HETEROGENOUS IMMUNOASSAY FOR CARDIAC MUSCLE TROPONIN cTNI ON A DIGITAL MICROFLUIDIC DEVICE. 681–683 (2013).

3. Li, Y., Baker, R. J. & Raad, D. A Highly Efficient and Reliable Electrowetting on Dielectric Device for Point-of-Care Diagnostics. (2015).

4. Lin, T., Yao, D., Lin, T. & Yao, D. Applications of EWOD Systems for DNA Reaction and Analysis Applications of EWOD Systems for DNA Reaction and Analysis. **4243,** (2012).

5. Taniguchi, T., Torii, T. & Higuchi, T. Chemical reactions in microdroplets by electrostatic manipulation of droplets in liquid media. *Lab Chip* **2,** 19–23 (2002).

6. Ding, H. *et al.* Accurate dispensing of volatile reagents on demand for chemical reactions in EWOD chips. *Lab Chip* **12,** 3331 (2012).

7. Wang, W., Chen, J. & Zhou, J. Droplet generating with accurate volume for EWOD digital microfluidics. *Proc. - 2015 IEEE 11th Int. Conf. ASIC, ASICON 2015* **m,** 8–11 (2016).

8. Wissman, J., Dickey, M. D. & Majidi, C. Field-Controlled Electrical Switch with Liquid Metal. *Adv. Sci.* **4,** (2017).

9. Kuiper, S. & Hendriks, B. H. W. Variable-focus liquid lens for miniature cameras. *Appl. Phys. Lett.* **85,** 1128–1130 (2004).

10. Heikenfeld, J. *et al.* Electrofluidic displays using Young-Laplace transposition of brilliant pigment dispersions. *Nat. Photonics* **3,** 292–296 (2009).

11. Chang, Y. H., Lee, G. Bin, Huang, F. C., Chen, Y. Y. & Lin, J. L. Integrated polymerase chain reaction chips utilizing digital microfluidics. *Biomed. Microdevices* **8,** 215–225 (2006).

12. Abdelgawad, M., Freire, S. L. S., Yang, H. & Wheeler, A. R. All-terrain droplet actuation. *Lab Chip* **8,** 672 (2008).

13. Cho, S. K., Moon, H. & Kim, C. Creating , Transporting , Cutting , and Merging Liquid Droplets by Electrowetting-Based Actuation for Digital Microfluidic Circuits. **12,** 70–80 (2003).

14. Cooney, C. G., Chen, C. Y., Emerling, M. R., Nadim, A. & Sterling, J. D. Electrowetting droplet microfluidics on a single planar surface. *Microfluid. Nanofluidics* **2,** 435–446 (2006).

15. Berthier, J. *Microdrops and digital microfluidics. William Andrew, Norwich, NY* (2008). doi:10.1016/B978-1-4557-2550-2.00012-2

16. Chakraborty, S. & Mittal, R. Droplet dynamics in a microchannel subjected to electrocapillary actuation Droplet dynamics in a microchannel subjected to electrocapillary actuation. **104901,** (2007).

17. Berthier, J. *et al.* Actuation potentials and capillary forces in electrowetting based microsystems. **134,** 471–479 (2007).

18. Yi, U. C. & Kim, C. J. Characterization of electrowetting actuation on addressable single-side coplanar electrodes. *J. Micromechanics Microengineering* **16,** 2053–2059 (2006).

19. Das, D., Das, S. & Biswas, K. Effect of Electrode Geometry on Voltage Reduction in EWOD Based Devices E f ysLdA Y '. 371–375 (2010).

20. Jain, V., Devarasetty, V. & Patrikar, R. Effect of electrode geometry on droplet velocity in open EWOD based device for digital micro fl uidics applications. *J. Electrostat.* **87,** 11–18 (2017).

21. Xu, X., Sun, L., Chen, L., Zhou, Z. & Xiao, J. Electrowetting on dielectric device with crescent electrodes for reliable and low-voltage droplet manipulation. **064107,** (2015).

22. Banerjee, A. N., Qian, S. & Joo, S. W. High-speed droplet actuation on single-plate electrode arrays. *J. Colloid Interface Sci.* **362,** 567–574 (2011).

23. Chang, J. H. & Pak, J. J. Twin-plate electrowetting for efficient digital microfluidics. *Sensors Actuators, B Chem.* **160,** 1581–1585 (2011).

24. Geng, H., Feng, J., Stabryla, L. M. & Cho, S. K. Dielectrowetting manipulation for digital microfluidics: creating, transporting, splitting, and merging of droplets. *Lab Chip* **17,** 1060–1068 (2017).

25. Ren, H., Fair, R. B., Pollack, M. G. & Shaughnessy, E. J. Dynamics of electro-wetting droplet transport. *Sensors Actuators, B Chem.* **87,** 201–206 (2002).

26. Dey, R., Ghosh, U. U., Chakraborty, S. & DasGupta, S. Dynamics of Electrically Modulated Colloidal Droplet Transport. *Langmuir* **31,** 11269–11278 (2015).

27. Ahmadi, A., Najjaran, H., Holzman, J. F. & Hoorfar, M. Two-dimensional flow dynamics in digital microfluidic systems. *J. Micromechanics Microengineering* **19,** 065003 (2009).

28. Quilliet, C. & Berge, B. Electrowetting: A recent outbreak. *Curr. Opin. Colloid Interface Sci.* **6,** 34–39 (2001).

29. Ward, C. A. & Wu, J. Effect of contact Line curvature on solid-fluid surface tensions without line tension. *Phys. Rev. Lett.* **100,** 1–4 (2008).

30. Ahmadi, A., Devlin, K. D. & Hoorfar, M. Numerical study of the microdroplet actuation switching frequency in digital microfluidic biochips. *Microfluid. Nanofluidics* **12,** 295–305 (2012).

31. Blake, T. D. The Physics of Moving Wetting Lines. 1–19

32. De Ruijter, M. J., Charlot, M., Voué, M. & De Coninck, J. Experimental evidence of several time scales in drop spreading. *Langmuir* **16,** 2363–2368 (2000).

33. Seveno, D. *et al.* Dynamics of wetting revisited. *Langmuir* **25,** 13034–13044 (2009).

34. Nelson, W. C. & Kim, C. C. J. Journal of Adhesion Science and Droplet Actuation by (EWOD): A Review. *J. Adhes. Sci. Technol.* **26,** 1747–1771 (2012).

35. Son, D. *et al.* NIH Public Access. **86,** 573–579 (2007).